Revisiting the five-decade-old structure of the Fe 2 WO 6 powder with incommensurate modulations

Éric Quarez, Julio César Espinosa-Angeles, Olivier Crosnier, Olivier Joubert, Thierry Brousse

▶ **To cite this version:**

Éric Quarez, Julio César Espinosa-Angeles, Olivier Crosnier, Olivier Joubert, Thierry Brousse. Revisiting the five-decade-old structure of the Fe 2 WO 6 powder with incommensurate modulations. CrystEngComm, 2021, 41 (23), pp.7298-7304. ⟨10.1039/d1ce00916h⟩. ⟨hal-03378437⟩

HAL Id: hal-03378437

https://hal.science/hal-03378437v1

Submitted on 29 Nov 2021

HAL is a multi-disciplinary open access archive for the deposit and dissemination of scientific research documents, whether they are published or not. The documents may come from teaching and research institutions in France or abroad, or from public or private research centers.

L'archive ouverte pluridisciplinaire **HAL**, est destinée au dépôt et à la diffusion de documents scientifiques de niveau recherche, publiés ou non, émanant des établissements d'enseignement et de recherche français ou étrangers, des laboratoires publics ou privés.

HAL Authorization

Revisiting the five-decade-old structure of the Fe_2WO_6 powder with incommensurate modulations

Éric QUAREZ[*a], Julio César ESPINOSA-ANGELES[ab], Olivier CROSNIER[ab], Olivier JOUBERT[a] and Thierry BROUSSE[ab]

a. Université de Nantes, CNRS, Institut des Matériaux Jean Rouxel, IMN, F-44000 Nantes, France

b. Réseau sur le Stockage Electrochimique de l'énergie (RS2E), FR CNRS 3459, CEDEX, 80039 Amiens, France

*E-mail: eric.quarez@cnrs-imn.fr

Abstract

Iron tungstate, Fe_2WO_6, is a promising photocatalytic, thermoelectric and electrochemically active material for energy storage devices. However, its structure is poorly described in the literature reporting on these applications. For the first time, we solved the crystal structure of the high temperature form using powder X-ray diffraction and the incommensurately modulated structural model. The structure adopts a (3 + 1)-dimensional *Pbcn*(0β0)000 superspace group with the cell parameters a = 4.57964(7) Å, b = 5.58662(8) Å, c = 4.96920(7) Å and the modulation vector q = 0.6687(4) b^*, close to the commensurate case q = 2/3 b^*. The first-order satellite reflections visible in powder diffraction patterns show, compared to the main reflections, a substantial broadening of the diffraction lines, caused by the small size of the ordered domains. This broadening has been successfully described by a line-broadening model, designed for incommensurately modulated structures, and confirms the incommensurate structural description. Such findings can be of great help to further understand the reported physical and electrochemical properties.

Introduction

The high temperature form of Fe_2WO_6 (so-called γ-Fe_2WO_6) is the most studied phase among the three polymorphs α,[1] β[2] and γ[3] mainly because it is relatively simple to synthesize. In 1974, it has been reported that the structure of γ-Fe_2WO_6 adopts the tri-α-PbO_2 structure-type with b axis thrice of that of α-PbO_2 ($a_{\alpha\text{-PbO2}}$, $3b_{\alpha\text{-PbO2}}$, $c_{\alpha\text{-PbO2}}$, *Pbcn* space group) with a = 4.576(2) Å, b = 16.766(5) Å, c = 4.967(2) Å.[3] The structure can be described as a cationic ordered α-PbO_2 structure in which two zigzag chains of edge-sharing octahedra, one containing Fe(1) cations and the other containing Fe(2) and W cations arranged alternately.[2] In general, knowledge of the detailed crystal structure of a material is the basis and prerequisite for further study of its physical properties. The γ-Fe_2WO_6 material has been studied in many fields for its electrical,[4] dielectric[5] and magnetic[6,7] properties. In terms of applications, γ-Fe_2WO_6 has been investigated as a negative electrode material for lithium-ion battery,[8–10] photoelectrode material for water oxidation,[11] visible-light photocatalyst[12] and n-type thermoelectric material.[13] Recently, our group tested Fe_2WO_6 as a potential negative electrode material in an electrochemical capacitor using a 5M $LiNO_3$ aqueous electrolyte. It showed interesting pseudocapacitive performance in terms of volumetric capacitance thanks to the high density of this oxide and long-term cycling behavior was achieved with such electrode.[14] For this latter purpose, Fe_2WO_6 sample was prepared using a polyol-mediated route at low temperature (220°C). A temperature-dependent X-ray diffraction study indicated, at 800°C, the formation of a well-crystallized phase whose diffraction peaks were successfully indexed into the cell of the α-PbO_2 structure ($a_{\alpha\text{-PbO2}}$, $b_{\alpha\text{-PbO2}}$, $c_{\alpha\text{-PbO2}}$, *Pbcn* space group). At 900 and 950°C, additional reflections appear corresponding to the tri-α-PbO_2 structure with the remarkable difference that these reflections are broader than the other reflections. In parallel, a Fe_2WO_6 sample was prepared by the classical ceramic route at 950°C and the same behavior was observed: some diffraction peaks, the same as those of the polyol sample, are broader than others. In order to shed light on this particular phenomenon, the structure of the polyol and ceramic powders at 900 and 950°C has been carefully investigated and reveals that the structure of γ-Fe_2WO_6 is perfectly described using the superspace formalism. The present article gives full details on the Rietveld refinement of the high-temperature form of γ-Fe_2WO_6 solved in a (3+1)D space group and provides an explanation of the physical origin of the reflection broadening.

2. Experimental

Synthesis

Polycrystalline samples of γ-Fe_2WO_6 were synthesized using the standard solid state reaction. The starting materials Fe_2O_3 (Riedel-de Haën, purity > 95 %) and WO_3 (Sigma-Aldrich, 99.9%) were mixed stoichiometrically and ground in an agate mortar. The powders were annealed at 950 °C for 24 h in air. To follow the effect of annealing on peak broadening in Fe_2WO_6 X-Ray powder patterns, several heat treatments of Fe_2WO_6 were performed at 950°C for 24 h with intermediate grinding and XRD recording. Samples of γ-Fe_2WO_6 phase were also prepared by a low temperature polyol-mediated route.[14] The resulting powders

were ground before undergoing two separate heat treatments in air at 900 and 950°C. The powders obtained by solid state reaction or by polyol route are hereafter referred to as ceramic and polyol samples.

Powder X-ray Diffraction

The XRD pattern of the ceramic samples was recorded in air at room temperature (RT) with a Bruker D8 A25 diffractometer using a Cu-*Kα*1-*Kα*2 radiation (*λ* = 1.54060, 1.54439 Å) and a LynxEye detector in Bragg-Brentano geometry. XRD patterns of the polyol samples were recorded in air at room temperature using a Bruker D8 Advance. Data were collected in the Bragg–Brentano geometry using a Cu-*Kα*1-*Kα*2 radiation (*λ* = 1.54060, 1.54439 Å) and a Vantec detector. XRDPs of the polyol samples were also recorded in air at room temperature (RT) in Bragg-Brentano geometry with a PANalytical X'Pert Pro diffractometer using a Cu-*Kα*1-*Kα*2 radiation (*λ* = 1.540598, 1.5444260 Å) and an X'Celerator detector. Le Bail and Rietveld analyses of the XRD data were performed using JANA2006[15] and the fundamental Cheary-Coelho approach for XRD profile parameters was applied in refinement for each diffractometer.[16] The estimated standard deviations of all refined parameters were calculated using Bérar & Lelann corrections.[17] A movie showing the incommensurately modulated Fe_2WO_6 structure was recorded using JANA2020.

3. Results and discussion

Preliminary structural refinements

The Figure 1 shows the XRPD performed at room temperature of the ceramic sample prepared at 950 °C and the polyol samples annealed at 900 or 950°C. All peaks can be indexed in the tri-α-PbO_2 structure-type cell (inset of Figure 1). At 950°C, the plots of the polyol and ceramic samples show narrower and broader diffraction lines highlighted by black and green *hkl* indices, respectively. It is interesting to note that the narrower diffraction lines have *hkl* indices following the rule *hkl*, *k* = 3n, n being an

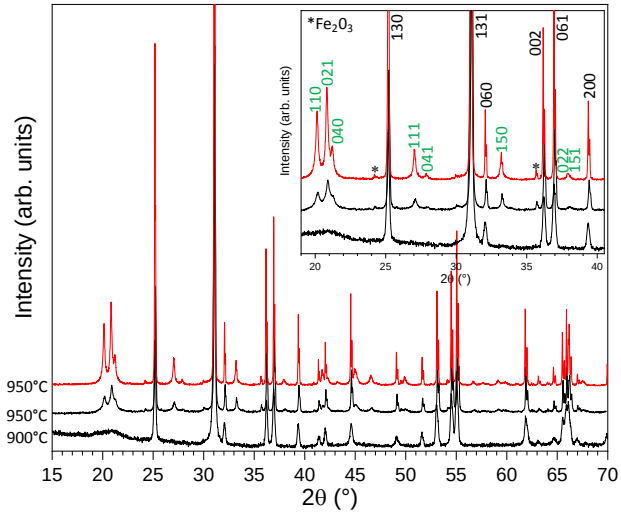

Figure 1. XRPD at room temperature of the ceramic sample synthesized at 950 °C (red) and the polyol (black) samples annealed at 900 or 950°C. The inset shows the *hkl* indexation considering *a* = 4.576(2) Å, *b* = 16.766(5) Å, *c* = 4.967(2) Å cell in a *Pbcn* space group.

integer. At 900°C, the plot of the polyol sample shows a large bump located around 20-22° corresponding to the 2θ positions of the strongest and broadest reflections in the ceramic plot. We expect that at 900 and 950°C, the structure of the sample is identical but the broad diffraction lines (for instance, 110, 021 and 040) in the 950°C plots are so broad that they appear as a large bump at 900°C and the least intense broad diffraction lines in the 95O°C plots (for instance, 111, 041, 150, 022 and 151) do not appear in the 900°C plot.

The structure of the ceramic sample was initially refined by the Rietveld method in the *Pbcn* space group using the model of γ-Fe_2WO_6,[3,6] with Fe atoms in two 4c sites (0,y,0.25) with y ≈ 0.06, y ≈ 0.72, W atoms in one 4c site (0,y,0.25) with y ≈ 0.39 and O atoms in three 8d sites. The refinement yielded non-positive definite atomic displacement parameters (ADP) for both Fe atoms and two O atoms. In addition, the use of anisotropic size or strain broadening parameters to try to model the broadening of some reflections was not successful. This is related to the unusual equation governing the *hkl* indices. The broader diffraction lines are the cause of the structural differences between the γ-Fe_2WO_6 sample reported by Senegas *et al.*[3] and the ceramic and polyol samples in the present study. It is interesting to note that $ZnNb_2O_6$, with the columbite structure ($3a_{\alpha\text{-PbO2}}$, $b_{\alpha\text{-PbO2}}$, $c_{\alpha\text{-PbO2}}$) was initially refined in a 3D model[18] but was recently solved in a (3+1)D model.[19] This encouraged us to solve and refine the structure of the ceramic and polyol samples in a (3+1)D model by applying the superspace formalism using JANA2006 software.[15]

Introduction to incommensurate structural refinement

In a 3+n D (n = 1, 2 or 3) spaces, the reciprocal space vectors are usually expressed as $H = ha^* + kb^* + lc^* + mq$ (a^*, b^*, and c^* are the basis vectors of the 3D reciprocal lattice). The modulation vector can be expressed as $q = \alpha\, a^* + \beta\, b^* + \gamma\, c^*$, where α, β, and γ are rational numbers for commensurate cases and irrational for incommensurate cases.

In the present study, the unit cell of γ-Fe_2WO_6 (a = 4.576(2) Å, b = 16.766(5) Å, c = 4.967(2) Å), which corresponds to a cationically ordered α-PbO_2 structure, is transformed into a cell without cation ordering, by dividing the parameter b by a factor of three, which leads to $a \approx 4.57$ Å, $b \approx 5.58$ Å and $c \approx 4.96$ Å. All observed XRPD reflections from the ceramic sample fulfilled the reflection conditions for the (3+1)D superspace group $Pbcn(0\beta0)000$.[20–22] The main reflections ($hklm$, $m = 0$) could be indexed on the basis of an orthorhombic unit cell ($a \approx 4.57$ Å, $b \approx 5.58$ Å and $c \approx 4.96$) and the satellite reflections ($hklm$, $m \neq 0$) could be indexed on the basis of a incommensurate modulation vector, q = 0.6687(4) b^*, where b^* is the reciprocal lattice vector. The β component of the modulation vector is close, but significantly different from the 2/3 (≈ 0.6667) rational ratio (difference > 5 $\sigma(\beta)$). Therefore, the structure should a priori be considered as incommensurate, an assumption later on confirmed by the refinements. The structure of γ-Fe_2WO_6 is thus a (3+1)-dimensional incommensurately modulated structure. In the (3+1)D superspace formalism approach, an additional coordinate x_4 can be expressed as $x_4 = t + q{\cdot}x$, where $x = (x_1, x_2, x_3)$ is the coordinate of physical-space with respect to the lattice and the parameter t ($0 \leq t \leq 1$) is the distance between a point and physical space.

Refinement of the incommensurately modulated Fe_2WO_6 structure

The results of the structural refinement are given in Table 1 and the details of the refined parameters of the final refinement are given in Table 2. Le Bail refinement of the modulated Fe_2WO_6 structure was performed in the $Pbcn(0\beta0)000$ superspace group starting with $\beta = 2/3$. The profile of main reflections was successfully described by a pseudo-Voigt function. The Rietveld refinement starts from the $ZnNb_2O_6$ model,[19] which is close to that of the α-PbO_2 structure, containing the following three atoms. Fe1 and W1 occupy the same site of multiplicity 4 (0,y,0.75) with $y \approx 0.16$ and O1 is located in a site of multiplicity 8 (x,y,z) with $x \approx 0.22$, $y \approx 0.11$, and $z \approx 0.41$. The parameters of Fe1 and W1 are restricted to have the same coordinates, modulations and ADP. First, the atomic positions and ADP are refined. A crenel function, describing the discontinuous occupation of the same site by Fe1 and W1 atoms, is then introduced in the refinement with x_4^0 (Fe1) = x_4^0 (W1) + 0.5 and Δ (Fe1), Δ (W1), according to the Fe_2WO_6 composition, equal to 2/3 and 1/3, respectively. After refinement, the main ($hklm$, $m = 0$) and the satellite reflections of order 1 ($hklm$, $m \pm 1$) are indexed. The refinement was further improved by introducing a displacive modulation function for the Fe1/W1 and O1 atoms and an anisotropic ADP for Fe1/W1 site.

Table 1. Crystallographic data, details of the data collection and structure refinement of Fe_2WO_6.

Chemical formula	$Fe_{2.667}W_{1.333}O_8$
Modulation	Incommensurate
Formula weight (g mol^{-1})	522.01
Crystal system	Orthorhombic
Super space group	$Pbcn(0\beta0)000$
Temperature (K)	293
a (Å)	4.57964(7)
b (Å)	5.58662(8)
c (Å)	4.96920(7)
V (Å^3)	127.136(3)
Modulation wave vector	q = 0.6687(4) b^*
Z	1
D_{calc} (g cm^{-3})	6.818
Radiation type	Cu $K\alpha$
Wavelength (Å) $K\alpha1$, $K\alpha2$, $I\,(K\alpha2)/I\,(K\alpha1)$	1.5406, 1.54439, 0.5
Diffractometer	Bruker D8 A25
2θ range (°), step scan (°), no. of data pts	10-100, 0.015, 6137
Profile function for main reflections	Pseudo-Voigt
No. of background parameters	12-term Legendre polynomials
No. of reflections (obs [I > 3σ(I)]/all)	184/201
No. of main reflections, $m = 0$ (obs/all)	63/68
No. of satellite reflections, $m \pm 1$ (obs/all)	121/133
Number of refined parameters	49
Rp (%)	7.92
wRp (%)	11.26
GoF (goodness of fit)	1.33
R, wR (%) (R_{obs}/R_{all})	3.81/4.17, 4.42/4.49
R, wR (%) (R_{obs}/R_{all}) main reflections	2.55/2.79, 3.13/3.22
R, wR (%) (R_{obs}/R_{all}) first-order satellites	5.94/6.45, 5.09/5.15
$\Delta\rho_{max}$ / $\Delta\rho_{min}$ (e Å^{-3})	2.09 / -2.19
Volume fraction Fe_2WO_6/Fe_2O_3	0.962(5)/0.037(5)

At this stage, the profile fitting of the satellite reflections is not satisfactory because the refinement does not take into account their broadening. A method, based on a line-broadening model, proposed by Leineweber & Petrıcek (2007),[23] designed for incommensurately modulated structures and successfully used in similar cases[24,25] was then applied. The refinement of the values of the twelve S'_{hklm} coefficients, describing the line-broadening in case of orthorhombic symmetry, leads to three S'_{hklm} coefficient values, S'_{2002}, S'_{2002} and S'_{0022}, significantly higher than the other S'_{hklm} coefficients, whose values are set to 0. The refinement leads to a substantial improvement in the reliability factors and the broadening of the satellite reflections is now correctly described (see the final Rietveld refinement plot displayed in Figure 2). Refining the β-value, by adding a single refined parameter, led to lower R-values compared to those obtained with the commensurate model. A small amount of Fe_2O_3 phase (< 4 vol. %) is present in the ceramic sample. Refinement tests considering the formula $Fe_{2-2x}^{3+}W_{1+x}^{6+}O_6$ with an equation linking Δ(Fe1) and Δ(W1) surprisingly resulted in an Fe-rich composition, which is the opposite of what is targeted. This test composition was abandoned and the stoichiometric composition Fe_2WO_6 was reapplied and considered as the final formula. The Figure 3 summarizes the different structural models tested and the final values of GoF and *wRp* obtained. For the model selected in this study (Fig. 3a), the blue line showing the difference between the calculated and experimental data is quite flat indicating an excellent structural model. The values of GoF and *wRp* are 1.33 and 11.26%, respectively. In the case of the commensurate case (Fig. 3b), the blue line is rougher, the GoF and *wRp* values are slightly higher (1.39 and 11.80%, respectively). When a line-broadening model is not considered in the refinements (Fig. 3c-d), the GoF and *wRp* values increase greatly, reaching 3.02 and 25.53% in the incommensurate case with first-order satellite reflections (Fig. 3c) and 3.14 and 26.55% with the addition of second-order satellite reflections (Fig 3d). Note that the use of a line-broadening model in the latter leads to GoF and *wRp* values of 1.44 and 12.17%, relatively higher than the values of the selected model. Figure S1a-f shows the occupational and positional modulations of Fe1, W1 and O1 atoms along the x_4 axis. Table S1 gives the selected interatomic distances in the Fe_2WO_6 ceramic sample and Figure 4 represents the detailed distributions of the Fe–O and W–O distances. The distances of the Fe-O and W-O bonds in the incommensurately modulated Fe_2WO_6 structure are in the range of standard values.

Table 2. Atomic coordinates and atomic displacement parameters (Å^2) obtained from the superspace refinement of the incommensurately modulated Fe_2WO_6 structure ((3+1)D group *Pbcn*(0β0)000, a = 4.57964(7) Å, b = 5.58662(8) Å, c = 4.96920(7) Å, V = 127.136(3) Å^3, q = 0.6687(4) b*)

Atom	Site multiplicity	x	y	z	U_{eq} [1] / U_{iso}
Fe1/W1	4	0	0.1678(5)	0.75	0.0206(6)[1]
O1	8	0.2234(17)	0.1163(14)	0.4178(15)	0.011(2)

Atom	U11	U22	U33	U12	U13	U23
Fe1/W1	0.0158(10)	0.0242(11)	0.0217(11)	0	0.001(2)	0

Parameters of the occupational wave using crenel function (x_4^0 and Δ are the center and the width of the wave along the x_4 axis, respectively).

Atom	x_4^0	Δ
Fe1	0.7604(17)	0.6667
W1	0.2604(17)	0.3333

Amplitudes of the displacive modulation function

Atom	xcos1	ycos1	zcos1	xsin1	ysin1	zsin1
Fe1/W1	0	0.0020(8)	0	0	-0.0044(9)	0
O1	-0.032(4)	-0.015(3)	0.000(6)	-0.013(4)	0.008(6)	0.014(3)

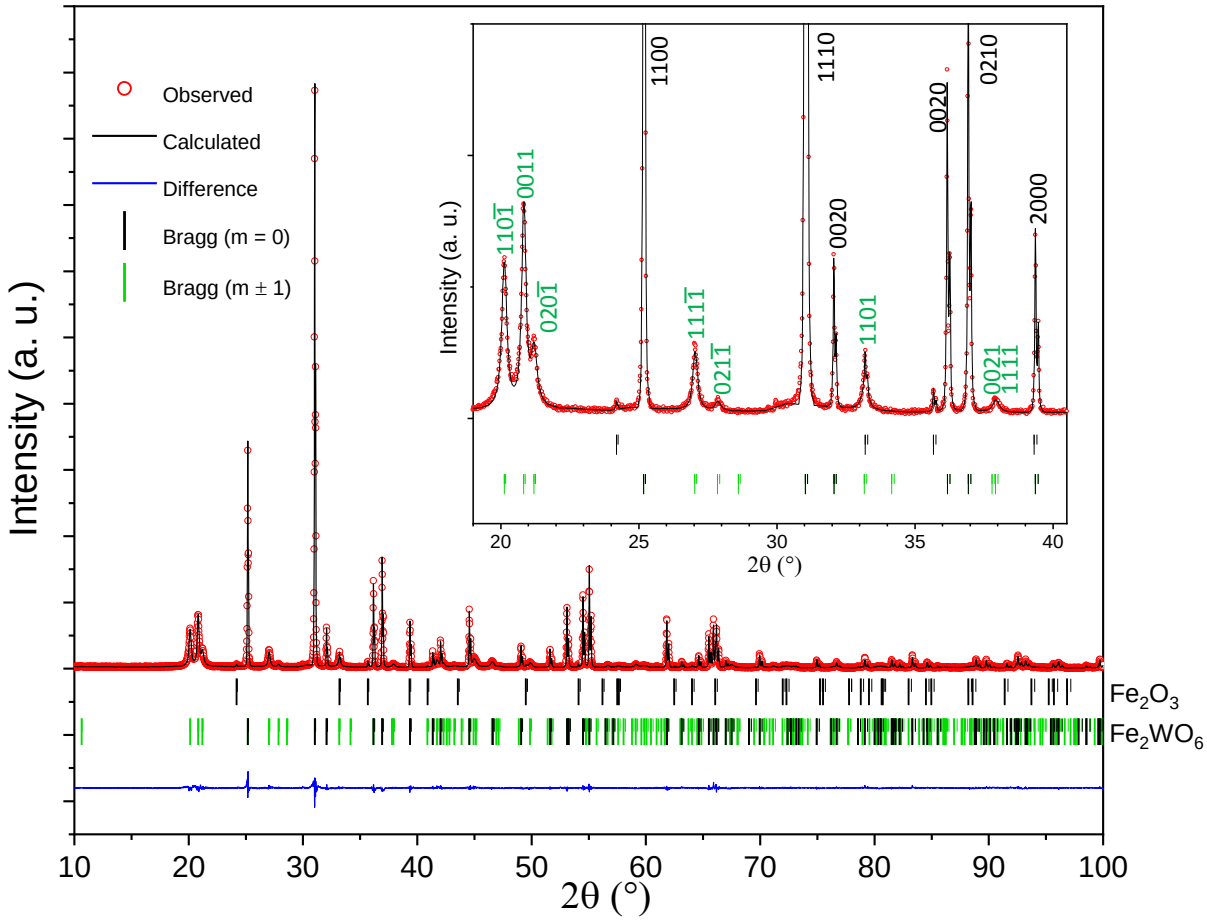

Figure 2. Final Rietveld refinement plot of the XRD data at RT of the Fe_2WO_6 ceramic sample with Cu-*Kα*1-*Kα*2 radiation.
The inset shows a portion of the pattern with indexation of the main and satellite reflections. Long and short ticks correspond to *Kα*1 and *Kα*2, respectively.

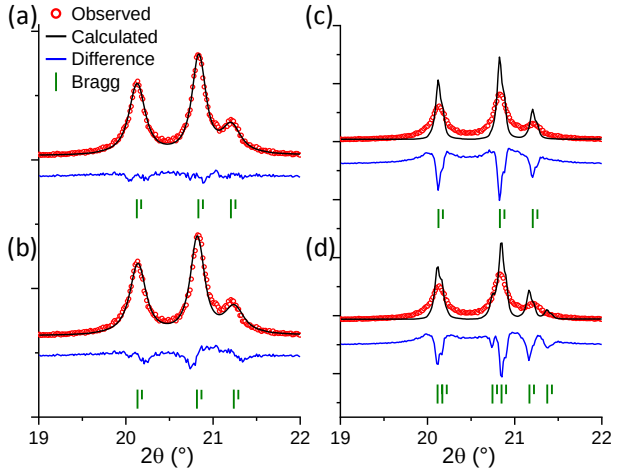

Figure 3. Portion of Rietveld refinement plots of room temperature XRD data of the Fe_2WO_6 ceramic sample illustrating broaden satellite reflections based on several structural models (a) incommensurate case, q = 0.6687(4), line-broadening model, GoF = 1.33, *wRp* = 11.26 %, which corresponds to the model selected in this study, (b) commensurate case, q = 2/3, line-broadening model, GoF = 1.39, *wRp* = 11.80 %, (c) incommensurate case, q = 0.6685(4), no line-broadening model, GoF = 3.02, *wRp* = 25.53 %, (d) incommensurate case, q = 0.6709(3), no line-broadening model, second-order satellite reflections considered in the refinement, GoF = 3.14, *wRp* = 26.55 %.

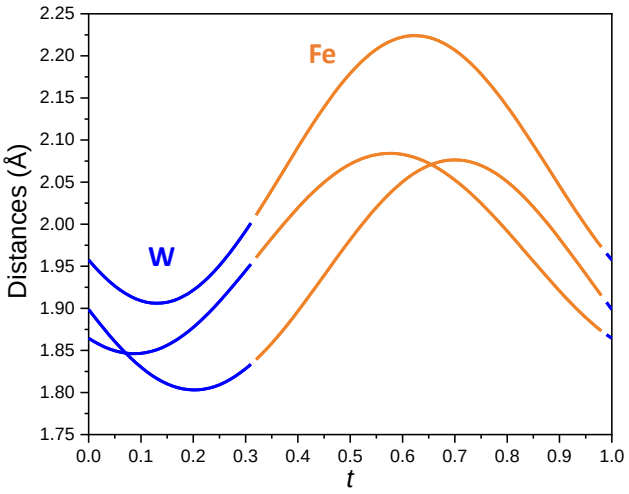

Figure 4. Evolution of W–O and Fe–O distances versus the internal parameter *t* of the Fe_2WO_6 ceramic sample.

Crystallite size of ordered domains in Fe_2WO_6 samples

For the XRDP of the ceramic sample, we are in the special case where, first, the line broadening occurs only for the satellite reflections, as the main reflections are narrow and, second, only the first-order (i.e. $m \pm 1$) satellite reflections are present on the pattern.[23–25] Therefore, variations in the q vector are mainly responsible for the broadening of the satellites observed in the experiment.[23] This result confirms the use of an incommensurate structural model to solve and refine the XRD plot of the Fe_2WO_6 ceramic powder.

The values of the refined parameters S'_{2002}, S'_{2002} and S'_{0022} could be related to the anisotropic size of the ordered domains in the Fe_2WO_6 samples.[23] The effective crystallite size D_x along the three crystallographic directions could thus be calculated[25] for the ceramic sample. The same calculations were carried out for the polyol samples heated to 900 or 950°C after performing similar Rietveld refinements. The results are summarized in Table 3. We observe that the β component deviates more from the rational value 2/3 in the polyol samples compared to the ceramic and conclude that the synthesis route has strong influence on this value. As expected, the effective crystallite sizes are highest for the ceramic sample, ranging from 200 to 500 Å, and lowest for the polyol sample heated to 900°C, ranging from 16 to 45 Å. The ceramic phase was then heat treated at 950°C, with intermediate grinding and XRPD, for a total of 100 h. The results show a continuous decrease in S' values associated with a continuous increase in domain size. The phase, ceramic or polyol annealed at 900 or 950°C, does not consist of one single domain but is composed from small, differently oriented domains. The limited size of these domains leads to a size-broadening of the satellite reflections. However, the main reflections are not broadened, because the basic structure of the differently oriented domains diffracts coherently. In later stages of annealing, the coarsening of the initially small ordered domains leads to a narrowing of the satellite reflections and an increase in the size of the domains.

Table 3. Peak profile parameters S'_{HKL2} for line broadening of satellite reflections and effective size D_x along the three crystallographic directions of Fe_2WO_6 ceramic sample heated at 950°C and polyol samples heated at 900 or 950°C. For each incommensurately modulated structure, the value of β in q = βb^* is given.

	Ceramic 950°C	Polyol 950°C	Polyol 900°C
β	0.6687(4)	0.670(3)	0.697(15)
S'_{2002} (°/Å^2)^2	13.35(19)	37(2)	3140(84)
S'_{0202} (°/Å^2)^2	14.9(3)	32(2)	277(25)
S'_{0022} (°/Å^2)^2	3.03(17)	17(2)	1569(47)
$D_{x\|\|a^*_{orth}}$(Å)	≈ 252	≈ 151	≈ 16
$D_{x\|\|b^*_{orth}}$(Å)	≈ 195	≈ 133	≈ 45
$D_{x\|\|c^*_{orth}}$(Å)	≈ 487	≈ 205	≈ 21

Cation ordering in Fe_2WO_6 samples

The Movie in the SI shows the 3D structure of the Fe_2WO_6 ceramic sample as a function of the internal t ($0 \le t \le 1$) parameter. When the parameter t varies from 0 to 1 values, the occupational modulations change the nature of the cations in the MO_6 octahedra and these are associated with the positional modulations that change the distances of the Fe-O and W-O bonds. When the M-O bond distances increase, the cation type changes from W to Fe and when the M-O bond distances decrease, the cation type changes from Fe to W, in agreement with the Shannon ionic radii.[26] In general, the cell is composed of one W cation and three Fe cations and there are few values of t for which two Fe atoms and two W atoms are present at the same time. This leads, by adding cell compositions at each t, to the final formula Fe_2WO_6. The modulated structure is significantly different from the reported γ-Fe_2WO_6 in which Fe and W atoms are ordered in zigzag chains of edge-sharing octahedra.

To go further and visualize the impact of the new structural description using the superspace formalism, from commensurate to incommensurate cases, on the ordering of the cations, we examine precisely the different structural models of the Fe_2WO_6 samples (Fig. 5). The structure published in 1974[3] is thus compared with the approximate 3D structures generated from the *Pbcn*(0β0)000 superspace group. In the *Pbcn* space group, the structure is described as the stacking along the *a* axis of layers consisting of zigzag chains of edge-sharing octahedra. In one layer, one-third of the zigzag chains contain FeO_6 octahedra and two-thirds of the chains consist of alternating FeO_6 and WO_6 octahedra (green delimiter in Fig. 5a). All layers are identical, with two consecutive layers being translated by a vector (1/2, 1/2, 0). In the *ab* plane, the layers are connected to each other by corner sharing with two columns of Fe octahedra alternating with one column of W octahedra (right panel). In a layer of the commensurate case (Fig. 5b), the sequence of zigzag chains is different in the *bc* plane: one-third is composed of WO_6 octahedra and two-thirds contain FeO_6 octahedra (red delimiter). In the incommensurate cases, the 3D cells generated from the *Pbcn*(0β0)000 superspace group with increasing value of the β component of the modulation vector, from 0.6687(4) to 0.697(15), are shown in Fig. 5(c-e). For the value closest to the 2/3 commensurate case (ceramic sample synthesized at 950°C, Fig. 5c), the layers are, in the *bc* plane, composed of red and green sequences. In the *ab* plane, a stacking defect is observed with a missing column of W octahedra (see blue arrow). As the value of the β component increases, the number of irregularities also increases. Thus, for β

= 0.670(3) (polyol sample heat treated at 950°C, Fig. 5d), the layers in the *bc* plane, as for the previous case, are composed of green and red sequences but the secondary layer, which is assumed to be identical to the first layer, a zigzag chain is different. Instead of being composed only of Fe octahedra, it consists of alternating FeO_6 and WO_6 octahedra (see red arrow). In the *ab* plane, a column of Fe octahedra is missing (orange arrow). Finally, for the value of β farthest from the 2/3 commensurate case (polyol sample heat treated at 900°C, Fig. 5e), the number of chain mismatch and stacking defects increases, highlighted by colored arrows. We can establish that the synthesis conditions and the temperature, through the subsequent heat treatments, have a direct influence on the β value of the modulation vector which plays an important role in the ordering of the cations in the Fe_2WO_6 samples.

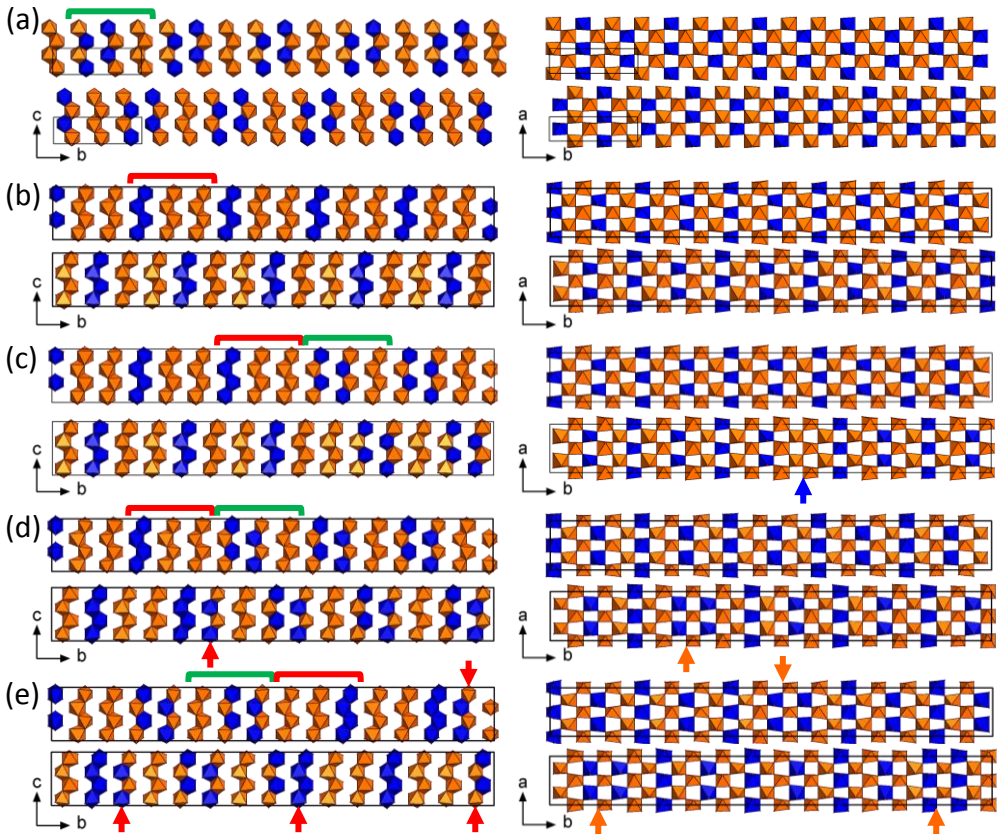

Figure 5. Representation of cation ordering in the *bc* (left panel) and *ab* (right panel) planes in Fe_2WO_6 samples considering different structural models. (a) 2x5x2 supercell in the *Pbcn* space group (b-e) 3D 2x15x2 supercells generated from the *Pbcn*(0β0)000 superspace group, commensurate case (b) $\beta = 2/3$, incommensurate cases (c) $\beta = 0.6687(4)$, (d) $\beta = 0.670(3)$ and (e) $\beta = 0.697(15)$. Color scheme: WO_6 octahedra, blue; FeO_6 octahedra, orange.

Conclusions

For the first time, we solved the powder structure of a promising material, Fe_2WO_6, prepared by two different synthesis methods and annealed at 900 or 950 °C. The phases exhibit an incommensurately modulated structure and crystallize in (3 + 1)D *Pbcn*(0β0)000 superspace group. The variation of the q value of the modulation vector broadens the satellite reflections, in comparison to the main reflections. This broadening is related to the small size of the ordered domains. The synthesis route has a strong influence on the q value and, by extension, the size of the ordered domains. The further the β component deviates from the commensurate value, the more the ordering of the cations is disturbed. This new structural description may help to better understand the properties of future research dealing with this material or similar compounds, especially with regards to the reported electrochemical properties.

References

1 C. Parant and J.-C. Bernier, *C R Acad Sc*, 1973, **276**, 495–497.
2 S. Caubergh, N. Matsubara, F. Damay, A. Maignan, F. Fauth, P. Manuel, D. D. Khalyavin, B. Vertruyen and C. Martin, *Inorg. Chem.*, 2020, **59**, 9798–9806.
3 J. Senegas and J. Galy, *J. Solid State Chem.*, 1974, **10**, 5–11.
4 N. Guskos, V. Likodimos, S. Glenis, S. K. Patapis, L. C. Palilis, J. Typek, M. Wabia and I. Rychlowska-Himmel, *Phys. Rev. B*, 1999, **60**, 7687–7690.
5 S. N. Panja, J. Kumar, L. Harnagea, A. K. Nigam and S. Nair, *J. Magn. Magn. Mater.*, 2018, **466**, 354–358.
6 H. Pinto, M. Melamud and H. Shaked, *Acta Crystallogr. A*, 1977, **33**, 663–667.
7 J.-J. Pak, M. Bahgat and M.-K. Paek, *J. Alloys Compd.*, 2009, **477**, 357–363.
8 E. Kendrick, A. Świątek and J. Barker, *J. Power Sources*, 2009, **189**, 611–615.
9 D. Saritha, *Mater. Today Proc.*, 2021, **38**, 2512–2514.
10 K. Xu, X. Shen, Z. Ji, A. Yuan, L. Kong, G. Zhu and J. Zhu, *Chem. Eng. J.*, 2021, **413**, 127504.
11 F. F. Abdi, A. Chemseddine, S. P. Berglund and R. van de Krol, *J. Phys. Chem. C*, 2017, **121**, 153–160.
12 S. B. Rawal, D. P. Ojha, S. D. Sung and W. I. Lee, *Catal. Commun.*, 2014, **56**, 55–59.
13 R. Schuler, T. Norby and H. Fjellvåg, *Phys. Chem. Chem. Phys.*, 2020, **22**, 15541–15548.
14 J. C. Espinosa-Angeles, N. Goubard-Bretesché, E. Quarez, C. Payen, M.-T. Sougrati, O. Crosnier and T. Brousse, *Nanomaterials*, 2021, **11**, 1405.
15 V. Petříček, M. Dušek and L. Palatinus, *Z. Für Krist. - Cryst. Mater.*, 2014, **229**, 345–352.
16 R. W. Cheary and A. A. Coelho, *J. Appl. Crystallogr.*, 1998, **31**, 851–861.
17 J.-F. Bérar and P. Lelann, *J. Appl. Crystallogr.*, 1991, **24**, 1–5.
18 M. Waburg and H. Müller-Buschbaum, *Z. Für Anorg. Allg. Chem.*, 1984, **508**, 55–60.
19 D. Zhao, F.-X. Ma, R.-J. Zhang, F.-F. Li, L. Zhang, J. Yang, Y.-C. Fan and X. Xin, *CrystEngComm*, 2016, **18**, 2929–2936.
20 T. Janssen, A. Janner, A. Looijenga-Vos and P. M. de Wolff., *Int. Tables Crystallogr. 2006 Vol C Ch 98*, 907–955.
21 H. T. Stokes, B. J. Campbell and S. van Smaalen, *Acta Crystallogr. A*, 2011, **67**, 45–55.
22 S. van Smaalen, B. J. Campbell and H. T. Stokes, *Acta Crystallogr. A*, 2013, **69**, 75–90.
23 A. Leineweber and V. Petricek, *J. Appl. Crystallogr.*, 2007, **40**, 1027–1034.
24 A. Arakcheeva, P. Pattison, G. Chapuis, M. Rossell, A. Filaretov, V. Morozov and G. Van Tendeloo, *Acta Crystallogr. B*, 2008, **64**, 160–171.
25 A. Leineweber, *J. Solid State Chem.*, 2009, **182**, 1846–1855.
26 R. D. Shannon, *Acta Crystallogr. Sect. A*, 1976, **32**, 751–767.